Editors' Suggestion

Engineering the Floquet spectrum of superconducting multiterminal quantum dots

Régis Mélin,[1] Romain Danneau,[2] Kang Yang,[3,4] Jean-Guy Caputo,[5] and Benoît Douçot[3]
[1]*Univ. Grenoble Alpes, CNRS, Grenoble INP, Institut Néel, 38000 Grenoble, France*
[2]*Institute of Nanotechnology, Karlsruhe Institute of Technology, D-76021 Karlsruhe, Germany*
[3]*Laboratoire de Physique Théorique et Hautes Energies, Sorbonne Université and CNRS UMR 7589, 4 place Jussieu, 75252 Paris Cedex 05, France*
[4]*Laboratoire de Physique des Solides, CNRS UMR 8502, Univ. Paris-Sud, Université Paris-Saclay F-91405 Orsay Cedex, France*
[5]*Laboratoire de Mathématiques, INSA de Rouen, Avenue de l'Université, F-76801 Saint-Etienne du Rouvray, France*

(Received 12 March 2019; published 31 July 2019)

Here we present a theoretical investigation of the Floquet spectrum in multiterminal quantum dot Josephson junctions biased with commensurate voltages. We first draw an analogy between the electronic band theory and superconductivity which enlightens the time-periodic dynamics of the Andreev bound states. We then show that the equivalent of the Wannier-Stark ladders observed in semiconducting superlattices *via* photocurrent measurements, appears as specific peaks in the finite frequency current fluctuations of superconducting multiterminal quantum dots. In order to probe the Floquet-Wannier-Stark ladder spectra, we have developed an analytical model relying on the sharpness of the resonances. The charge-charge correlation function is obtained as a factorized form of the Floquet wave function on the dot and the superconducting reservoir populations. We confirm these findings by Keldysh Green's function calculations, in particular regarding the voltage and frequency dependence of the resonance peaks in the current-current correlations. Our results open up a road map to quantum correlations and coherence in the Floquet dynamics of superconducting devices.

DOI: 10.1103/PhysRevB.100.035450

I. INTRODUCTION

Since the early 1960's, the Josephson effect has attracted continuous interest and its development over the years has led to major applications in quantum information and technologies. It occurs when two superconductors connect a non-superconducting material and its physical mechanism can be described *via* the notion of Andreev bound states (ABS). These phase-sensitive midgap doublets are produced by proximity effect. The ABS microscopically originate from the formation of entangled electron-hole pairs in the normal conductor and can be seen as two-level systems [1]. Many physical properties of the Josephson junctions, such as the value of the Josephson current, depend on the energy-phase relation of the ABS at zero bias voltage and finite phase drop across the junction [2–5].

The growing interest in quantum information has boosted investigations on the zero-energy states in proximitized superconducting structures [6]. ABS physics is pivotal in the interpretation of the experimental evidence for Majorana bound states in nanowires [7–11]. Moreover, new states of matter based on ABS have been predicted in conventional superconductor multiterminal devices, offering the possibility to engineer artificial topological materials featuring Weyl singularities [12–15]. We note that recent works aiming at probing these topological systems have been reported [16,17]. Experiments on multiterminal superconducting junctions have been already performed [18–20], highlighting multiple Andreev reflections (MAR) involving more than two leads [21–23] as well as correlations between Cooper pairs [24–28]. In addition, ABS in the static regime have also been proposed to create triplet correlations using ferromagnetic wires in multiterminal configurations [29], to study the effect of spin-orbit interactions in one-dimensional (1D) systems coupled to superconducting leads [30], and to simulate Andreev molecules using two Josephson junctions in series [31].

ABS have been experimentally studied by tunnel or microwave spectroscopy [32–43]. Theoretically, one can distinguish between two different regimes: the first one refers to a static phase configuration, i.e., when a Josephson junction is driven by a time-independent magnetic flux within a loop, with all parts of the circuit at the same chemical potential. The second one corresponds to a dynamical control of the superconducting phases, for instance when the system is set out-of-equilibrium *via* voltage biasing. The latter is a time-periodic problem and therefore described by the Floquet theory where time periodicity plays the role of spatial periodicity for electrons in a solid. Recently [44], some of the authors have shown that, set out of equilibrium, the ABS appear as periodic resonances equivalent to the Wannier-Stark ladders predicted [45] for a solid under electric field, and observed in semiconducting superlattices from photocurrent experiments [46,47]. In these superconducting systems, the time-periodicity of the ABS dynamics implies the emergence of a spectrum made of two sets of energy levels, namely the Floquet-Wannier-Stark (FWS) ladders.

In this paper, we study the Floquet spectrum of a superconducting multiterminal quantum dot (QD) by means of analytical and numerical calculations. We show that in this configuration (see Fig. 1) the FWS ladders can be revealed by finite frequency noise spectroscopy, with sharp peaks at the transitions between pairs of FWS resonances. Our

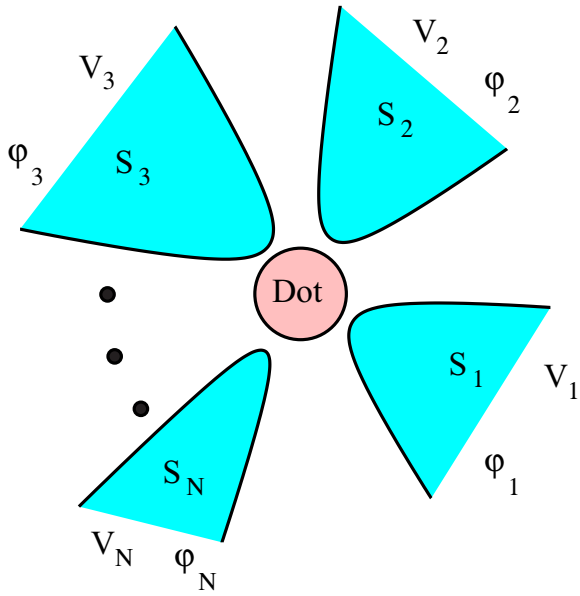

FIG. 1. A N-terminal superconducting-quantum dot biased at voltages $V_1, \ldots, V_N$. The superconducting phase of lead S_n evolves according to $\varphi_n(t) = \varphi_n + 2eV_n t/\hbar$, where $\varphi_1, \ldots, \varphi_N$ are the phases at the origin of time $t = 0$. Commensurate ratio between the V_n is assumed in the paper. The resonant quantum dot hosts a single spin-degenerate level at zero energy.

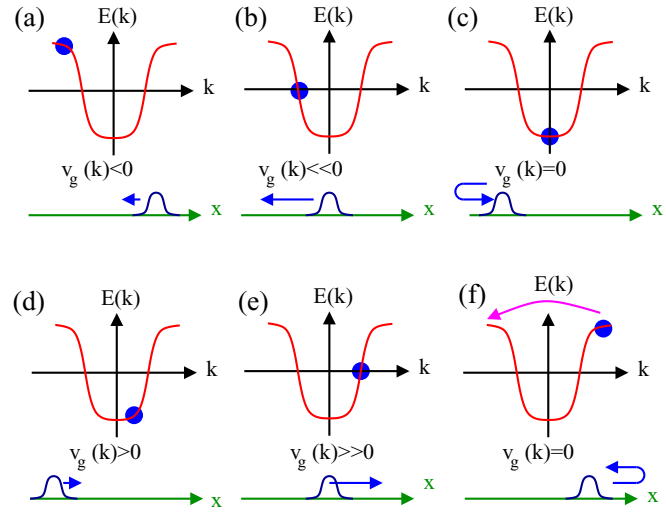

FIG. 2. Bloch oscillations. Evolution of wave vector k and real space coordinate x in Bloch oscillations. Wave vector k increases linearly in time according to $dk/dt = -eE/\hbar$, with E the electric field. The group velocity $v_g(t) = dE/dk$ oscillates as a function of time t, yielding oscillations of wave packets in real space, with frequency proportional to the electric field E. (a)–(f) cover one period of oscillations. Due to the periodicity of the lattice potential in real space, the Fourier point π/a_0' in (f) is identified to $-\pi/a_0'$ in (a).

approach involves an analytical calculation of the charge-charge correlation function which shows that the peak frequencies obtained in the noise match the energy spacing between arbitrary levels in the Floquet spectra. The analytical model based on a sharp resonance approximation is used to label the noise spectra obtained numerically from microscopic Keldysh Green's function calculations. Our work enables further investigations of the coherent qu-bit-like dynamics of two FWS ladders.

This paper is organized as follows. In Sec. II, we expose an analogy between Wannier-Stark ladders in band theory and in multiterminal hybrid superconducting systems. The results on the connection between the FWS resonance spectra and finite frequency cross-correlations are presented in Sec. IV. Summary and perspectives are provided in Sec. V.

II. PARALLEL BETWEEN BAND THEORY AND SUPERCONDUCTIVITY

Following the seminal works of Anderson [48,49], a classical parallel is known between two distinct fields of condensed matter physics, i.e., band theory and superconductivity. We go beyond by implementing this analogy for time-periodic Floquet Hamiltonians.

Bloch oscillations in periodic crystals. A simple cubic lattice crystal is parameterized by the spacing a_0 between nearest-neighboring sites. Electrons are localized independently on each atom if a_0 is much larger than the size of the atomic electronic clouds. As a_0 diminishes, the ground state degeneracy for the single-electron Hamiltonian is gradually lifted upon increasing tunnel coupling between neighboring electronic clouds. A "band" of energy with continuous spectrum is then formed in the thermodynamic limit. This corresponds to band theory with Bloch wave functions [50]. Eigenstates are extended plane waves multiplied by a function which is periodic in a_0.

In the presence of an additional static and uniform electric field E, Zener [51] showed theoretically that an electron in a crystal oscillates periodically in space, and that electromagnetic radiation is emitted at the corresponding frequency (see Fig. 2). However, the so-called Bloch oscillations have never been demonstrated experimentally for bulk materials (neither bulk metals nor bulk semiconductors). In this case, the inelastic scattering time is much shorter than the delay $\Delta t = h/eEa_0$ for crossing the Brillouin zone under action of electric field. However, Δt is strongly reduced in artificial semiconducting superlattices, in which the potential can be modulated with period a_0', much larger than the lattice parameter a_0 of a bulk semiconductor. The semiconducting superlattice Brillouin zone (having a size $\sim 1/a_0'$) is thus strongly reduced compared to that of the corresponding bulk semiconductor (having a size $\sim 1/a_0$). The delay for crossing the semiconducting superlattice Brillouin zone under action of the electric field can advantageously be much smaller than the inelastic scattering time [52]. Many cycles of Bloch oscillations are then possible on time scale much shorter than the inelastic scattering time, making possible the observation of Bloch oscillation-related effects. Bloch oscillations are the time-dependent counterpart of the Wannier-Stark ladder spectrum mentioned in Introduction. Indeed, the spectral gap eEa_0 between two consecutive energy levels in such ladder is equal to $h\nu_B$, where $\nu_B = 1/\Delta t$ is the frequency associated to Bloch oscillations. This has been observed in ultracold atoms [53–55]. We notice the properties of Bloch oscillations have

TABLE I. Analogy between band theory and superconductivity.

Band Theory	Superconductivity
Wave vectors	Superconducting phases
Position x_n in real space	Number N of transmitted Cooper pairs
x_n/a_0 integer equivalent to $2\pi/a_0$-periodic wave vector k	N integer equivalent to 2π-periodic phase φ
Plane waves in Bloch theory $\|k\rangle = \sum_x \exp(ikx)\|x\rangle$	States with fixed superconducting phase $\|\varphi\rangle = \sum_N \exp(iN\varphi)\|N\rangle$
Hopping between neighboring tight-binding sites	Transferring pairs between leads by Andreev reflection
Electric field $dk/dt = -eE$	Josephson relation $d\varphi_n/dt = 2eV_n/\hbar$
Wannier-Stark ladders	Floquet-Wannier-Stark ladders

already been used in Coulomb blockaded Josephson junction circuits for low noise amplification [56,57].

Parallel between band theory and superconductivity. The use of conventional superconductors (such as aluminum) in electronic devices based on the Josephson effect is at the heart of the developments on quantum circuits and quantum technologies. One of the reasons why superconductivity remains forefront in both fundamental and applied physics research for more than a century is reflected in the existence of broken gauge symmetry. The BCS microscopic theory describes superconductivity as an effect of electron-phonon coupling yielding formation of bound states of electron pairs with opposite spins, so-called "Cooper pairs," which condense into a collective ground state. Anderson implemented his theory of gauge invariance which successfully accounts for the Meissner effect on the basis of the so-called Higgs mechanism [48,49]. Even if the phase of a single superconductor is not measurable, phase differences are gauge-invariant (and thus measurable) quantities. Consequently, the Josephson effect occurs as a dissipationless current flowing through a weak link [58] connected by two phase biased superconductors.

It turns out that band theory and superconductivity share deep common features. Based on the concept of phase rigidity [48], Anderson has described the wave function associated to the Josephson effect as coherent superposition between states with different numbers of pairs within the two superconducting leads [49]. In solid state physics, wave vectors in the Brillouin zone are analogous to superconducting phases between 0 and 2π while the "position" basis corresponds to the "number of transmitted pairs" basis in superconductivity. The Wannier-Stark ladders emerge in both cases as natural consequence of this analogy. The parallel between band theory and superconductivity is described in Table I.

Having emphasized this analogy, it is worth pointing out a distinction between momentum k in band theory and the phase difference φ in superconductivity. Whereas k has to be regarded as a *good quantum number*, φ is a *classical parameter* in the BCS mean-field Hamiltonian. However, one can circumvent this issue by promoting φ to a genuine quantum degree of freedom, canonically conjugate to the number of transmitted Cooper pairs N (see Table I).

It turns out that superconductivity is not required for producing dynamical Wannier-Stark ladders [59]. In this work [59], the authors study theoretically the response of a semiconducting superlattice to a periodic train of pulses of the electric field. However, superconductivity offers the unique opportunity to explore Floquet physics with purely dc-voltage biasing.

How to detect FWS ladders? In a two-terminal Josephson junction biased with voltage V, the superconducting phase $\varphi(t)$ winds in time t according to the Josephson relation

$$\varphi(t) = \varphi + 2eVt/\hbar. \tag{1}$$

Then, the two equilibrium ABS [see Fig. 3(a)] give rise to two alternating FWS ladders [see Fig. 3(b)] [44], which are the counterparts of the Wannier-Stark ladders [45] observed experimentally in semiconducting superlattices [46,47].

This raises the natural question of how to demonstrate experimentally the presence of FWS ladders, and to extract their precise location in energy. The two ladders are indeed at energies (see Fig. 3)

$$E_{q,\pm} = E_\pm + qeV/\hbar \tag{2}$$

(q being an even integer for our two-terminal junction, and with any parity for three terminals). The simple relation $E_+ = -E_-$ for the energy shifts $E_\pm$ is valid in general. Far from crossing in the real part of FWS resonances, we have in addition $E_+ \simeq \langle E_{ABs}\rangle$, where $\langle E_{\rm ABS}\rangle$ is the average of the equilibrium ABS energy over the fast superconducting phase variable [44].

Microwave radiation can excite transitions between two arbitrary rungs E_{q_1,ϵ_1} or $E_{q_2,\epsilon 2}$ [see Eq. (2), with q replaced by q_1 or q_2, and $\epsilon_{1,2} = \pm$], on the condition of resonance $\Omega = E_{q_2,\epsilon_2} - E_{q_1,\epsilon_1}$ between the rf-field frequency Ω and the energy difference $E_{q_2,\epsilon_2} - E_{q_1,\epsilon_1}$ [see Eq. (2)], as illustrated by the drawing on Fig. 3(b). It is also possible to perform such spectroscopy by measuring current correlations at finite frequency, as it will be further explained in Sec. IV. There, we will show that, as a function of the measurement frequency Ω, the finite frequency current cross-correlations $S_{a,b}(\Omega)$ exhibit peaks at $\Omega = \Delta E_{+,p},\ \Delta E_{0,p},\ \Delta E_{-,p}$, with

$$\Delta E_{+,p} = E_{q_2,+} - E_{q_1,-} = E_+ - E_- + peV/\hbar, \tag{3}$$

$$\Delta E_{0,p} = E_{q_2,\epsilon} - E_{q_1,\epsilon} = peV/\hbar, \tag{4}$$

$$\Delta E_{-,p} = E_{q_2,-} - E_{q_1,+} = E_- - E_+ + peV/\hbar, \tag{5}$$

where $\epsilon = \pm$, and $p = q_2 - q_1$ is an even integer in the case of two terminals, but takes any parity for three-terminal systems with commensurate dc-voltage biasing, such as opposite voltages $V_a = -V, V_b = V$ and $V_c = 0$ in the quartet configuration [25]. Thus $\Delta E_{+,p}$ and $\Delta E_{-,p}$ encode interladder transitions, while $\Delta E_{0,p}$ corresponds to intraladder transitions.

III. HAMILTONIANS

We consider in the paper a QD coupled to N superconducting reservoirs (see Fig. 1). The reservoirs are assumed to be biased at dc voltages V_i ($1 \leqslant i \leqslant N$) (chosen to be commensurate). Therefore we write $V_i = s_i V$ where s_i is an integer. For example, in the quartet configuration [25], we have $N = 3$,

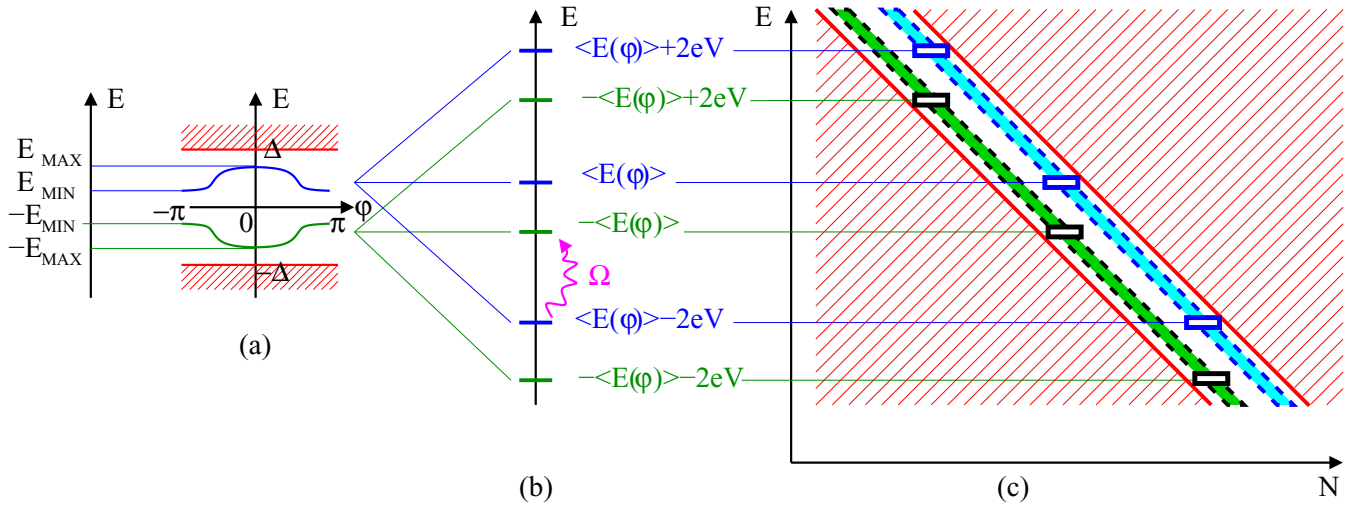

FIG. 3. Floquet-Wannier-Stark ladders. (a) Energies $\pm E(\varphi)$ of the two ABS as a function of superconducting phase variable φ in absence of bias voltage ($V = 0$). The red dashed regions correspond to the quasiparticle continua. (b) The corresponding Floquet-Wannier-Stark ladders in presence of finite bias voltage V. Notation $\langle E(\varphi)\rangle$ is used for the average of $E(\varphi)$ over the superconducting phase variable φ. (c) Energy vs number N of transmitted Cooper pairs displaying the tilted band picture of Floquet-Wannier-Stark ladder localization.

and $s_i \in \{0, 1, -1\}$. It is easy to specialize to the two-terminal case, simply by setting to zero the tunneling coupling J_c to the reservoir such that $s_c = 0$. Then the dc voltage drop between the two remaining superconducting reservoirs is equal to $2V$.

The Hamiltonian can be written as

$$\mathscr{H}(t) = \mathscr{H}_0 + \mathscr{H}_J(t), \tag{6}$$

where $\mathscr{H}_0$ is an usual BCS Hamiltonian for the superconducting reservoirs and $\mathscr{H}_J(t)$ describes the tunneling processes between these reservoirs and the QD. Specifically,

$$\mathscr{H}_0 = \sum_{j=1}^{N}\sum_{\sigma}\int \frac{d^D\mathbf{k}}{(2\pi)^D}(\epsilon(j,\mathbf{k})c_\sigma^\dagger(j,\mathbf{k})c_\sigma(j,\mathbf{k}) + \Delta_j c_\uparrow^\dagger(j,\mathbf{k})c_\downarrow^\dagger(j,-\mathbf{k}) + \Delta_j^* c_\downarrow(j,-\mathbf{k})c_\uparrow(j,\mathbf{k})) \tag{7}$$

and

$$\mathscr{H}_J = \sum_{j=1}^{N} J_j \sum_{\sigma}\int \frac{d^D\mathbf{k}}{(2\pi)^D}(e^{-is_j\omega_0 t}c_\sigma^\dagger(j,\mathbf{k})d_\sigma + e^{is_j\omega_0 t}d_\sigma^\dagger c_\sigma(j,\mathbf{k})). \tag{8}$$

Here, $c_\sigma^\dagger(j,\mathbf{k})$ and $c_\sigma(j,\mathbf{k})$ are creation and annihilation operators for an electron on reservoir j with momentum $\mathbf{k}$ and spin σ along the quantization axis. Corresponding operators on the dot are denoted by $d_\sigma^\dagger$ and d_σ. The dimension D of the reservoirs is left undetermined, since its actual value is not crucial. The basic frequency ω_0 is associated to single electron tunneling processes, and it is equal to $\omega_0 = eV/\hbar$. Note that $\omega_0 = \omega_J/2$, where ω_J is the Josephson frequency associated to V.

IV. RESULTS

The "sharp resonance" approximation is first introduced at moderately low voltage in Sec. IV A. In the next Sec. IV B, an analytical expression of the finite frequency charge-charge correlations is obtained with this sharp resonance approximation. Numerical results for the finite frequency current-current correlations are presented next in Sec. IV C.

A. Sketch of the sharp resonance approximation

The goal of this section is to develop an approximation scheme to evaluate analytically the resolvent $\mathscr{R}(E)$ at energy E, defined as

$$\mathscr{R}(E) = (E - \mathscr{H})^{-1}, \tag{9}$$

where the Hamiltonian $\mathscr{H}$ is given in Sec. III [see Eqs. (6)-(8)]. The resulting compact form of $\mathscr{R}(E)$ resulting from the sharp resonance approximation will be used in Sec. IV B to provide an analytical expression for the finite frequency charge-charge correlation function.

Break junction experiments realize superconducting weak links with only a few conduction channels [60–62]. In a single-channel weak link [63], the ABS are at energies $\pm\Delta$ if the phase bias $\varphi = 0$ vanishes, whatever contact transparency (with Δ the superconducting gap). Once biased at voltage V, the superconducting phase difference evolves in time according to Eq. (1). Consequently, the ABS touch periodically the gap edge singularities at energies $\pm\Delta$ in the presence of bias voltage: the narrow equilibrium ABS acquire large width at nonequilibrium. Indeed, numerical calculations [61] of the first harmonics of the current in a superconducting weak link show smooth energy dependence, without sharp resonances (see Figs. 3 and 4 in Ref. [61]).

The situation is quite different in superconducting-QD where the equilibrium ABS stay away from the gap edge singularities in the full range of the superconducting phase difference φ, even if $\varphi = 0$. Indeed, the ABS energies at $\varphi = 0$ are of order $\approx\Gamma$, with $\Gamma = J^2/W$. (In this expression, J is the hopping matrix element between the QD and the superconductor, and W the band-width of the superconducting leads. In experiments [19], the parameter Γ is usually a

fraction of the superconducting gap Δ). In a voltage-biased superconducting-QD, the equilibrium ABS are separated from the gap edge singularities by the finite energy difference $\approx \Delta - \Gamma$. Still, at finite V, the FWS resonances remain coupled by MAR to the semi-infinite quasiparticle continua. The resulting linewidth broadening $\gamma \approx \Delta \exp(-c\Delta/eV)$ is exponentially small in the ratio between the gap Δ and the voltage energy eV [28] [with c a constant of order unity]. Since γ drops rapidly to zero as Δ/eV is increased above unity, another mechanism of relaxation has to be advocated at inverse voltages larger than $3 \lesssim \Delta/eV$, such as the coupling to phonons [44].

Given the exponential dependence on inverse voltage of the MAR linewidth broadening γ, we discuss now (within the wave-function approach introduced in Sec. I of Ref. [64]) an approximation relying on the sharpness of the FWS resonances for $3 \lesssim \Delta/eV$ (see Secs. I– III in Ref. [64] for details). A central role in these calculations is played by $\mathscr{R}(E)$ in Eq. (9) which can be factorized according to

$$\mathscr{R}(\tilde{E} + p\omega_0)_{m,n} \simeq \sum_{\alpha=\pm} \frac{\Psi_{m+p}(E_\alpha) \otimes \Phi_{n+p}(E_\alpha)}{\tilde{E} - E_\alpha + i\Gamma_\alpha}, \tag{10}$$

where p is an integer. Eq. (10) above is identical to Eq. (18) in Sec. II of Ref. [64]. Further details on its demonstration can be found in Appendix A of Ref. [64]. The notation $\{\Psi_m(E)\}_{m\in\mathbb{Z}}$ stands for the two-component right zero-eigenvector of the Floquet equations. The notation $\{\Phi_n(E)\}_{n\in\mathbb{Z}}$ is used for the corresponding left eigenvector of the transposed equations. The notation $\tilde{E} + p\omega_0$ stands for the energy, where $\omega_0 = eV$ and E_α is the energy shift of the FWS ladder $\alpha = \pm$ [see Eq. (2)]. The notation Γ_α is used for the corresponding linewidth broadening.

B. Finite frequency charge-charge correlation function in the sharp resonance approximation

Now, we demonstrate Eqs. (3)–(5) in the sharp resonance approximation, on the example of the charge-charge correlation function

$$C(t,t') = \sum_{\sigma,\sigma'} \langle d^\dagger_\sigma(t) d_\sigma(t) d^\dagger_{\sigma'}(t') d_{\sigma'}(t')\rangle - \left(\sum_\sigma \langle d^\dagger_\sigma(t) d_\sigma(t)\rangle\right)\left(\sum_{\sigma'} \langle d^\dagger_{\sigma'}(t') d_{\sigma'}(t')\rangle\right), \tag{11}$$

where d_σ and $d^\dagger_\sigma$ are defined in the Appendix.

The sharp resonance approximation discussed above in the preceding Sec. IV A leads to simple expressions for (i) the charge-charge correlation function given by Eq. (11) (see below), (ii) the dot propagators (see Sec. II in Ref. [64]), (iii) the charge on the quantum dot (Sec. III in Ref. [64]), and (iv) the direct currents (see Sec. IV, again in Ref. [64]). Our analytical calculations can be also extended straightforwardly to the finite frequency current cross-correlations (the expression of which is not given here), however with more tedious formula.

Equation (11) is first Fourier transformed from times t, t' to frequencies ω, ω'. The resulting $C(\omega,\omega')$ has nonvanishingly small elements if $\omega - \omega'$ is an integer multiple of ω_0. Here, we limit the analysis to the "diagonal" time-translational invariant part of the finite frequency charge correlation function $C_d(\Omega) \equiv C(\Omega,\Omega)$, which takes the following form in the sharp resonance approximation (similar to Eqs. (24) and (25) in Ref. [64]):

$$C_d(\Omega) = 4 \sum_{i,j=1}^{N} \sum_{\alpha=\pm} \sum_{\beta=\pm} \sum_{p}^{(i,j)} \times \frac{S_{i,\alpha} S_{j,\beta} (\Gamma_\alpha + \Gamma_\beta)}{(\Omega - E_\alpha - E_\beta - p\omega_0)^2 + (\Gamma_\alpha + \Gamma_\beta)^2} \times \sum_{(m,m')\in\mathbb{Z}^2}^{(i,j)} F_{\alpha,\beta}(m,m',m-p,m'-p), \tag{12}$$

with

$$S_{i,\alpha} = \frac{\mathscr{A}_D J_i^2}{2(2\pi)^{D-1}\Gamma_\alpha} \sum_{p\in\mathbb{Z}} \sum_\tau \nu(i,\alpha,p,\tau)(k(i,\alpha,p,\tau))^{D-1} \times \theta(E_\alpha + p\omega_0 - |\Delta_i|)|\Phi(E_\alpha)_{-s_i+p,u} e^{i\varphi_i/2} \times x(i,k(i,\alpha,p,\tau)) - \Phi(E_\alpha)_{s_i+p,v} e^{-i\varphi_i/2} y(i,k(i,\alpha,p,\tau))|^2 \tag{13}$$

and

$$F_{\alpha,\beta}(m,m',n,n') = \Psi_{m,u}(E_\alpha)\Psi^*_{m',u}(E_\alpha)\Psi_{n,v}(E_\beta)\Psi^*_{n',v}(E_\beta) + \Psi_{m,v}(E_\alpha)\Psi^*_{m',u}(E_\alpha)\Psi_{n,u}(E_\beta)\Psi^*_{n',v}(E_\beta), \tag{14}$$

where the expression of $S_{i,\alpha}$ in Eq. (13) above coincides with Eq. (25) in Ref. [64]. The right and left "Floquet wave functions" are denoted by Ψ and Φ [see Eq. (9) above]. The Heaviside step function is denoted by θ in Eq. (13). The superconducting leads have dimension D in Eqs. (12)–(14). The notation $\mathscr{A}_D$ stands for the D-dimensional sphere area ($\mathscr{A}_1 = 2$, $\mathscr{A}_2 = 2\pi$, $\mathscr{A}_3 = 4\pi$). The integers s_i are used for characterizing commensurate voltage biasing: The voltage V_i on superconducting lead S_i is given by $V_i = s_i V$ (see also Appendix). The variable J_i is the tunneling amplitude between the quantum dot and the superconducting lead S_i phase φ_i. The integer p in Eq. (12) has the same parity as $s_i + s_j$, and m and m' have the same parity as s_i.

The BCS quasiparticle dispersion relation in lead j is given by

$$E(j,k) \equiv \sqrt{\epsilon(j,k)^2 + |\Delta_j|^2} = E_\alpha + p\omega_0, \tag{15}$$

where $\epsilon(j,k)$ is the kinetic energy. Eq. (15) has two solutions labeled by $\tau \in \{>,<\}$. The density of states $\nu(j,\alpha,p,\tau)$ is defined as follows:

$$\nu(j,\alpha,p,\tau) = \left[\frac{dE(j,k)}{dk}(k = k(j,\alpha,p,\tau))\right]^{-1}. \tag{16}$$

The notations x and y in Eq. (13) stand for the BCS coherence factors

$$x(j,\mathbf{k}) = \sqrt{\frac{1}{2}\left(1 + \frac{\epsilon(j,\mathbf{k})}{E(j,\mathbf{k})}\right)}, \tag{17}$$

$$y(j,\mathbf{k}) = \sqrt{\frac{1}{2}\left(1 - \frac{\epsilon(j,\mathbf{k})}{E(j,\mathbf{k})}\right)}. \tag{18}$$

In the expression (12) of the charge-charge correlation function in the sharp resonance approximation, α labels the two FWS ladders, and not all values of m, m', p, p' ranging from $-\infty$ to $+\infty$ contribute to a physically observable resonance in $C_d(\Omega)$. The "wave functions" $\Psi_{m,w}(E_\alpha)$ $(w = u, v)$ have indeed finite extent as a function of m, due to localization on the FWS ladders plotted as a function of the number of transmitted Cooper pairs [see Fig. 3(c)]. Further investigations on the extent of the FWS ladders as a function of N in the semiclassical limit will be presented elsewhere.

In general, Eq. (10) is the sum of two terms because of the summation over $\alpha = \pm$, but one of these can be discarded if the energy $\tilde{E} \approx E_\alpha$ is close to E_α. Then, the resolvent is well approximated by the resonant term in Eq. (10), which takes a simple factorized form involving products of the Ψ and Φ wave functions. The resulting expression Eq. (12) of the charge-charge correlation function is also factorized into the corresponding Φ and Ψ contributions: (i) the $S_{i,\alpha}$ (and $S_{j,\beta}$) factors given by Eq. (13) depend only on Φ, and they encode the contributions of the lead i (or j) populations to the resonance α (or β); (ii) The Ψ terms in the "form factors" $F_{\alpha,\beta}$ originate directly from Wick theorem for products of four-fermion operators, and they do not depend on the populations in the reservoirs.

Another appealing feature of Eq. (12) is that the frequency dependence solely encoded in a "minimal" information about (i) the spectrum of resonances (such as the energies E_α, the widths Γ_α) and (ii) the wave function $\Psi_m(E_\alpha)$ at resonance. The $S_{i,\alpha}$ coefficients contain indeed all information about the stationary state, and they reflect the initial state of the reservoirs before adiabatic switching of tunneling processes.

Further semiclassical analysis reveals that the sum over p in Eq. (13) converges easily since the decay of $\Phi(\tilde{E})_p$ at large p is very fast. We note that, besides this large p behavior, the factor $\nu(j, \alpha, p, \tau)$ diverges when $E_\alpha + p\omega_0$ is close to $|\Delta_j|$. The sum in Eq. (13) is then dominated by the contribution of quasiparticle states injected on the dot at energies close to the BCS gaps in the reservoirs.

A direct consequence of the compact Eq. (12) is emergence of three series of sharp peaks in $S_{a,b}(\Omega)$ at frequencies

$$\Omega_{\alpha,\beta,p} = E_\alpha + E_\beta + p\omega_0, \tag{19}$$

which coincide with the preceding Eqs. (3)–(5). The sign of these peaks depends on the Floquet wave functions, and thus, it cannot be predicted from simple arguments.

Now, we want to confirm these predictions from independent microscopic Keldysh Green's functions calculations for the finite frequency current-current correlation function. We also want to visualize the frequency-Ω and voltage-eV dependencies of the cross-correlations, with a choice of the model parameters compatible with possible experimental realization.

C. Numerical results for the cross-correlation spectra

In this section, we present our numerical results on the connection between the FWS ladders of resonances and the symmetrized finite frequency current-current cross-correlations $S_{a,b}(\Omega)$. After the necessary definition of $S_{a,b}(\Omega)$, the Floquet spectra are presented for the four sets of device parameters which will be used afterwards in the evaluation of $S_{a,b}(\Omega)$.

TABLE II. The couplings (a)–(d) used in the numerical calculations. [The same labeling (a)–(d) is used in Figs. 4–7]. The notation Γ_i (with $i = a,\ b,\ c$) stands for $\Gamma_i = J_i^2/W$, where J_i is the hopping amplitude between the dot and lead S_i, and W is the band-width of the superconductors.

Panel label	Number of terminals	Γ_a/Δ	Γ_b/Δ	Γ_c/Δ	$\varphi_q/2\pi$
(a)	2	0.3	0.3	0	
(b)	2	0.4	0.2	0	
(c)	3	0.3	0.3	0.3	0
(d)	3	0.3	0.3	0.3	0.1

Expression of $S_{a,b}(\Omega)$. The quantity $S_{a,b}(\Omega)$ calculated numerically is the diagonal term (in frequency) of the Fourier transform of the following two-time current-current correlation function

$$S_{a,b}(t, t') = \langle \delta\hat{I}_a(t)\delta\hat{I}_b(t')\rangle + (t \leftrightarrow t'), \tag{20}$$

where $\hat{I}_a(t)$ and $\hat{I}_b(t')$ are the operators for the currents entering superconducting leads S_a and S_b at times t and t'. The notations $\delta\hat{I}_a(t) = \hat{I}_a(t) - \langle\hat{I}_a(t)\rangle$ and $\delta\hat{I}_b(t') = \hat{I}_b(t') - \langle\hat{I}_b(t')\rangle$ are used for the deviations with respect to the expectation value in the stationary states.

The four sets of device parameters. Different configurations of the superconducting-QD (e.g., depending on the number of terminals, the symmetry of the contacts and the presence/absence of quartet phase [25] for three terminals) lead to qualitatively different variations in the voltage dependence of the Floquet spectra. All numerical calculations presented below were indeed carried out with the four sets of parameters labeled by (a)–(d) in Table II. The notation φ_q in this table stands for the so-called "quartet phase" [25], corresponding to the static phase combination appearing in a three-terminal Josephson junction biased with commensurate voltages. Indeed, the superconducting phase $\varphi_i(t)$ of leads S_i (with $i = a, b, c$) is given by $\varphi_i(t) = \varphi_i + 2eV_i t/\hbar$. With opposite voltage biasing in the three-terminal configurations (c) and (d) (i.e., $V_a = -V_b = V$ and $V_c = 0$), the static combination [25] φ_q is given by $\varphi_q = \varphi_a + \varphi_b - 2\varphi_c \equiv \varphi_a(t) + \varphi_b(t) - 2\varphi_c(t)$.

The rescaled spectra are shown in Fig. 4, where the x axis is Δ/eV (inverse voltage normalized to the gap) and y axis is E_n/eV (the FWS resonance energies divided by voltage). Indeed, Eqs. (3)–(5) for the Floquet levels lead to

$$\frac{E_{q,\pm}}{eV} = \frac{E_\pm}{eV} + q. \tag{21}$$

These plots in reduced variables [65] (i.e., E/eV versus Δ/eV) can advantageously be used instead of the more conventional ones (i.e., E/Δ versus V/Δ) in order to produce regular patterns of avoided levels at low voltage.

Figure 4 shows the FWS resonance energies E_n/eV evaluated from the maxima in $|\mathscr{R}(E)|$ [see Eq. (9)]. In addition to the expected FWS resonances, spurious maxima at energies E_m^* are visible in the small-Δ/eV region of the spectra. Inspection of the numerical data for the energy dependence of $|\mathscr{R}(E)|$ shows that they appear in the vicinity of the gap edges,

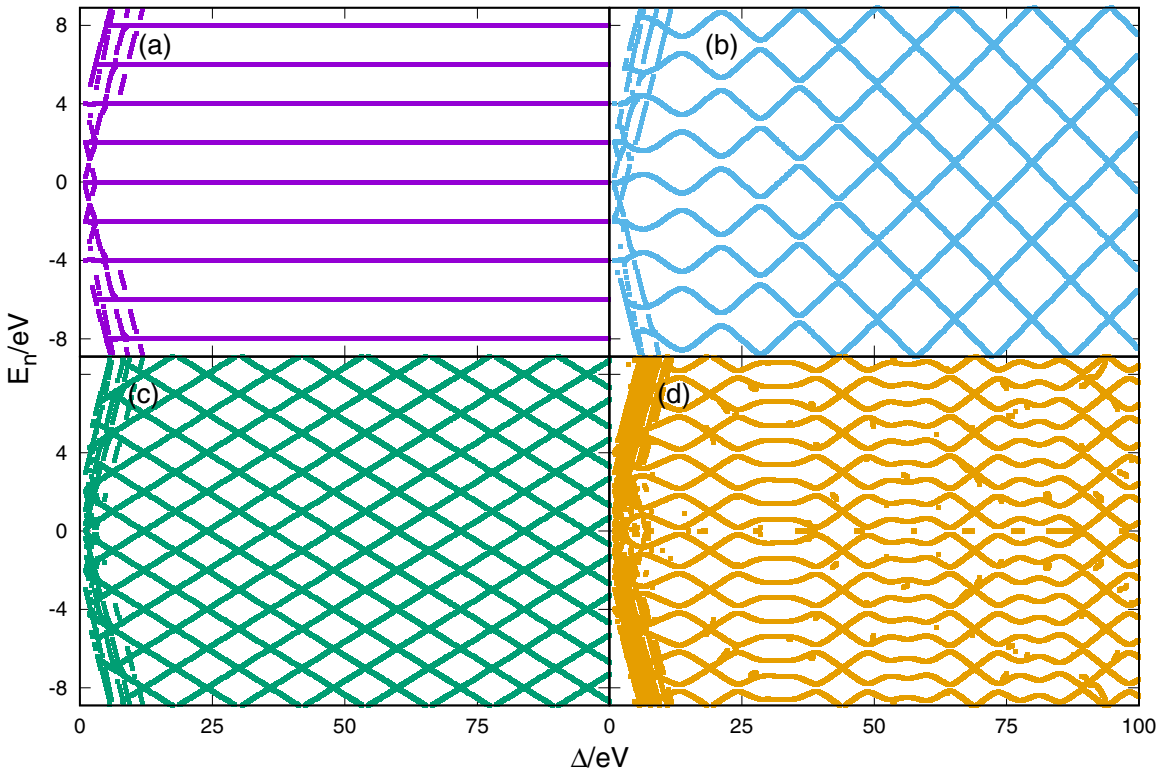

FIG. 4. Floquet-Wannier-Stark ladders. The figure shows the Floquet energies as a function of inverse voltage, using the rescaled variables given by Eq. (21). The x axis is Δ/eV and y axis is E/eV. Small voltage means large value of Δ/eV on x axis. The superconducting-QD junction parameters are given in Table II: (a) two symmetrically coupled terminals, $\Gamma_a/\Delta = \Gamma_b/\Delta = 0.3$; (b) two terminals with generically different couplings to the leads, $\Gamma_a/\Delta = 0.4$, $\Gamma_b/\Delta = 0.2$; (c) three symmetrically coupled terminals with vanishingly small quartet phase $\varphi_q/2\pi = 0$, $\Gamma_a/\Delta = \Gamma_b/\Delta = \Gamma_c/\Delta = 0.3$; and (d) three symmetrically coupled terminals with finite value for the quartet phase $\varphi_q/2\pi = 0.1$, $\Gamma_a/\Delta = \Gamma_b/\Delta = \Gamma_c/\Delta = 0.3$. As discussed in the text, the spurious data-points for $\Delta/eV \lesssim 10$ are an artifact of the gap edge singularities.

generally with tiny curvature $|d^2|\mathscr{R}(E_m^*)|/dE^2|$ compared to the sharp FWS resonances.

Very different behavior emerges on panels (a)–(d) of Fig. 4, according to the symmetry of the coupling between the dot and the leads (see Table II). For instance, the basic period on Fig. 4(b) with two terminals is $4eV/\hbar$, instead of $2eV/\hbar$ for three terminals [see Figs. 4(c) and 4(d)]. In this case, the Bogoliubov-de Gennes equations (see Sec. I in Ref. [64]) decouple into two blocks. Each of these blocks gives rise to a pair of FWS ladders, with the basic period $\Delta E = 4eV/\hbar$. This explains the period doubling observed in panels (a) and (b) of Fig. 4.

Another characteristic feature of these spectra of resonances is absence of level repulsion in Figs. 4(a) and 4(c). For these highly symmetric configurations of the tunnel amplitudes between the quantum dot and the superconducting leads, the Bogoliubov-de Gennes Hamiltonian commutes with the σ^x Pauli matrix, thus we get two decoupled tight-binding problems in the Floquet coordinate (e.g., the coordinate N on the x axis of Fig. 3). This explains why we do not observe Landau-Zener transitions [66,67] because the two FWS ladder are independent in Figs. 4(a) and 4(c). In this case, Bohr-Sommerfeld quantization [44] becomes exact for a single band, and $E_\pm = \pm\langle E_{\rm ABS}\rangle$, where $E_{\rm ABS}$ is the average of the equilibrium ABS energy over the fast phase variable. We have $\pm\langle E_{\rm ABS}\rangle = 0$ for the parameters on Fig. 4 (a), in agreement with the horizontal lines seen on this figure.

The spectra shown in Figs. 4(b) and 4(d) are more complex, since they both exhibit repulsion among FWS resonances. For panel (d), the two tunneling paths for Landau-Zener transitions [instead of a single one for panel (b)] produce a modulation of the level repulsion pattern related to Landau-Zener-Stückelberg interferences [67].

Numerical results for the cross-correlation spectra. Once Fourier transformed, Eq. (20) is written as a sum of terms originating from Wick theorem for products of four creation or annihilation operators in the current-current correlation function. Each of these terms is given by products of Keldysh Green's functions [22,28]. The latter can be expressed in terms of the resolvent defined by Eq. (9). This is formally similar to the superconducting quantum point contact [68] relevant to break-junction experiments [69]. In our calculations of the current-current cross-correlations in superconducting-QD, the numerical method relies on recursive Green's functions in energy, combined to sparse matrices algorithms, and adaptive integration over the spectral parameter [22,28]. The numerical value of the cross-correlations converges towards the exact answer upon increasing the adjustable level of accuracy.

Figure 5 shows the current-current cross-correlations $S_{a,b}(\Omega)$ [see Eq. (20)] as a function of frequency Ω, for

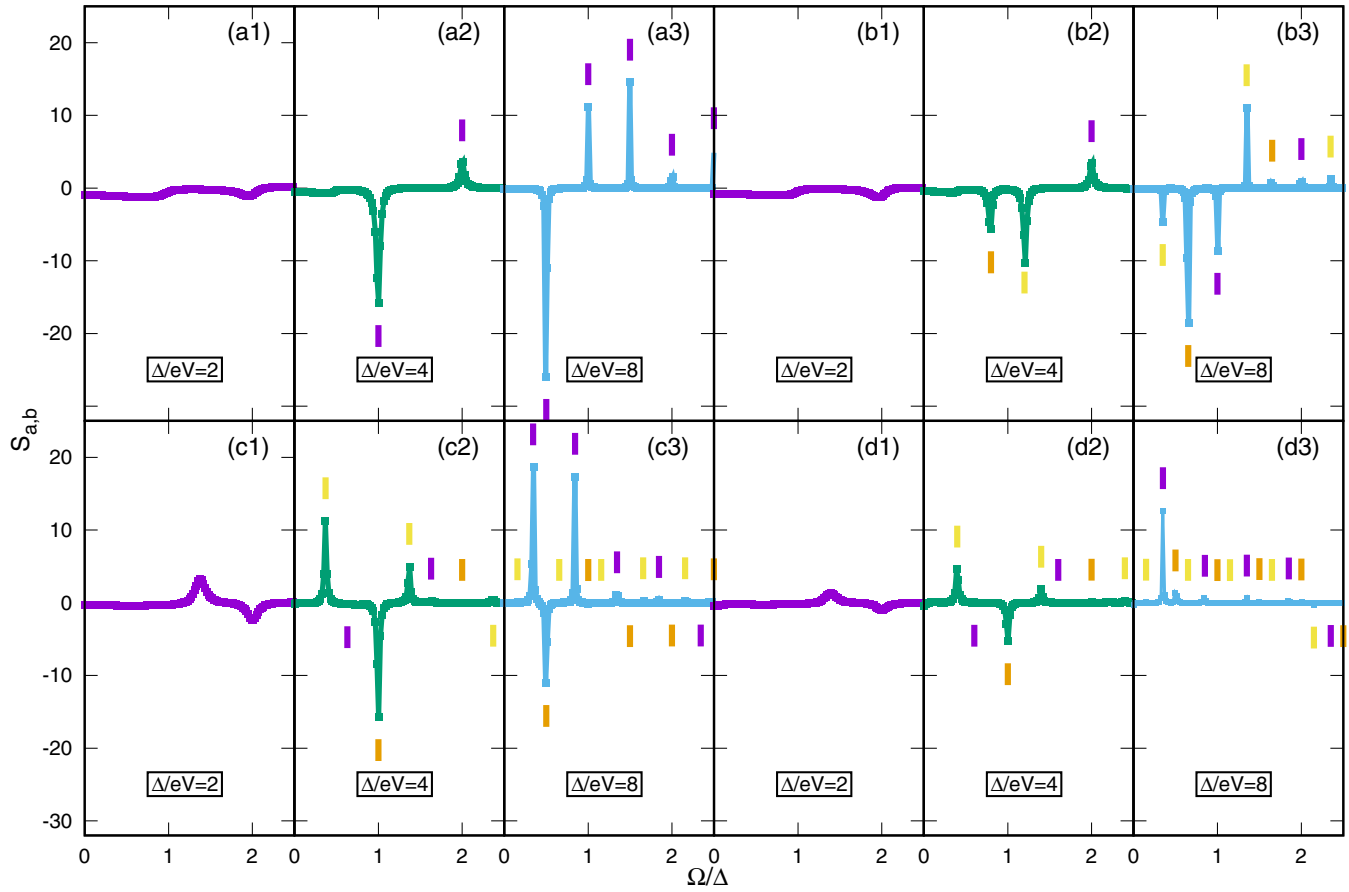

FIG. 5. Cross-correlation spectra $S_{a,b}(\Omega)$. The contact transparencies are given in Table II: [(a1), (a2), and (a3)] two symmetrically coupled terminals, $\Gamma_a/\Delta = \Gamma_b/\Delta = 0.3$; [(b1), (b2), and (b3)] two terminals with generically different couplings to the leads, $\Gamma_a/\Delta = 0.4$, $\Gamma_b/\Delta = 0.2$; [(c1), (c2), and (c3)] three symmetrically coupled terminals with vanishingly small quartet phase $\varphi_q/2\pi = 0$, $\Gamma_a/\Delta = \Gamma_b/\Delta = \Gamma_c/\Delta = 0.3$; and [(d1), (d2), and (d3)] three symmetrically coupled terminals with finite value for the quartet phase $\varphi_q/2\pi = 0.1$, $\Gamma_a/\Delta = \Gamma_b/\Delta = \Gamma_c/\Delta = 0.3$. The values of inverse voltage are indicated on the figure: ([a1), (b1), (c1) and (d1)] $\Delta/eV = 2$; [(a2), (b2), (c2), and (d2)] $\Delta/eV = 4$; and [(a3), (b3), (c3), and (d3)] $\Delta/eV = 8$. The theoretical prediction [see Eqs. (3)–(5)] for the collection of values of $E_n - E_m$ (i.e., the differences between Floquet energies) is shown by colored bars on each panel. Each bar x-axis coordinate is at the value of $E_n - E_m$. The color code is the following: yellow, magenta, and orange correspond to $\Delta E_{+,p}$, $\Delta E_{0,p}$, and $\Delta E_{-,p}$ respectively [see Eqs. (3)–(5)]. The x axis is Ω/Δ and y axis is $S_{a,b}$ in natural units. Temperature is vanishingly small.

the four sets (a)–(d) of junction parameters in Table II. The following values of inverse-voltage are used: $\Delta/eV = 2$ [panels (a1), (b1), (c1), and (d1)], $\Delta/eV = 4$ [panels (a2), (b2), (c2), and (d2)], and $\Delta/eV = 8$ [panels (a3), (b3), (c3), and (d3)]. In agreement with the preceding Sec. IV A, sharp peaks emerge on Fig. 5 for $S_{a,b}(\Omega)$, which become denser and narrower [44] as Δ/eV is increased (i.e., as voltage is reduced). It was verified that the zero-frequency limit $S_{a,a}(0)$ of the current-current autocorrelation function is always positive in these calculations, and that the zero-frequency cross-correlation $S_{a,b}(0)$ is negative for two terminals. The peaks in the frequency dependence of the cross-correlations $S_{a,b}(\Omega)$ (see Fig. 5) show both positive or negative sign, depending on the values of frequency or bias voltage. Indeed, inspection of Eqs. (12)–(14) reveals that the sign and amplitude of the resonances in $S_{a,b}(\Omega)$ cannot be fixed by a simple general rule. Instead, it depends on complex combinations of the Floquet wave functions which are oscillating as a function of the coordinate N in Fig. 3.

Figure 6 shows the same data as Fig. 5, but now the y axis (i.e., the $S_{a,b}$ axis) is on a logarithmic scale. This reveals many peaks, which disappear for frequencies $3 \lesssim \Omega/\Delta$.

The theoretical prediction for the three families of FWS transition energies $\Delta E_{+,p}$, $\Delta E_{0,p}$, and $\Delta E_{-,p}$ [see Eqs. (3)–(5)] are shown as bars of different colors in Figs. 5 and 6. The values of E_+ and E_- in Eq. (2) are calculated numerically from the sharp maxima in the resolvent $|\mathscr{R}(E)|$ [see Eq. (9)]. For clarity, the values of the y-axis (i.e., the $S_{a,b}$ or $\log_{10}|S_{a,b}|$-axis) coordinate of all bars has been shifted by a positive or negative offset.

The x-axis (i.e., the Ω-axis) coordinate of the bars (in Figs. 5 and 6) compares well with the location in energy of the sharp maxima in $S_{a,b}(\Omega)$ (see Fig. 5) or $\log_{10}|S_{a,b}(\Omega)|$ (see Fig. 6). This provides numerical evidence for the expectation (discussed above in the preceding section II) that the peak frequencies match the energy differences $E_n - E_m$ between pairs of Floquet states [see also the preceding Eq. (19) deduced from Eqs. (11)–(14)]. We note that a few of the

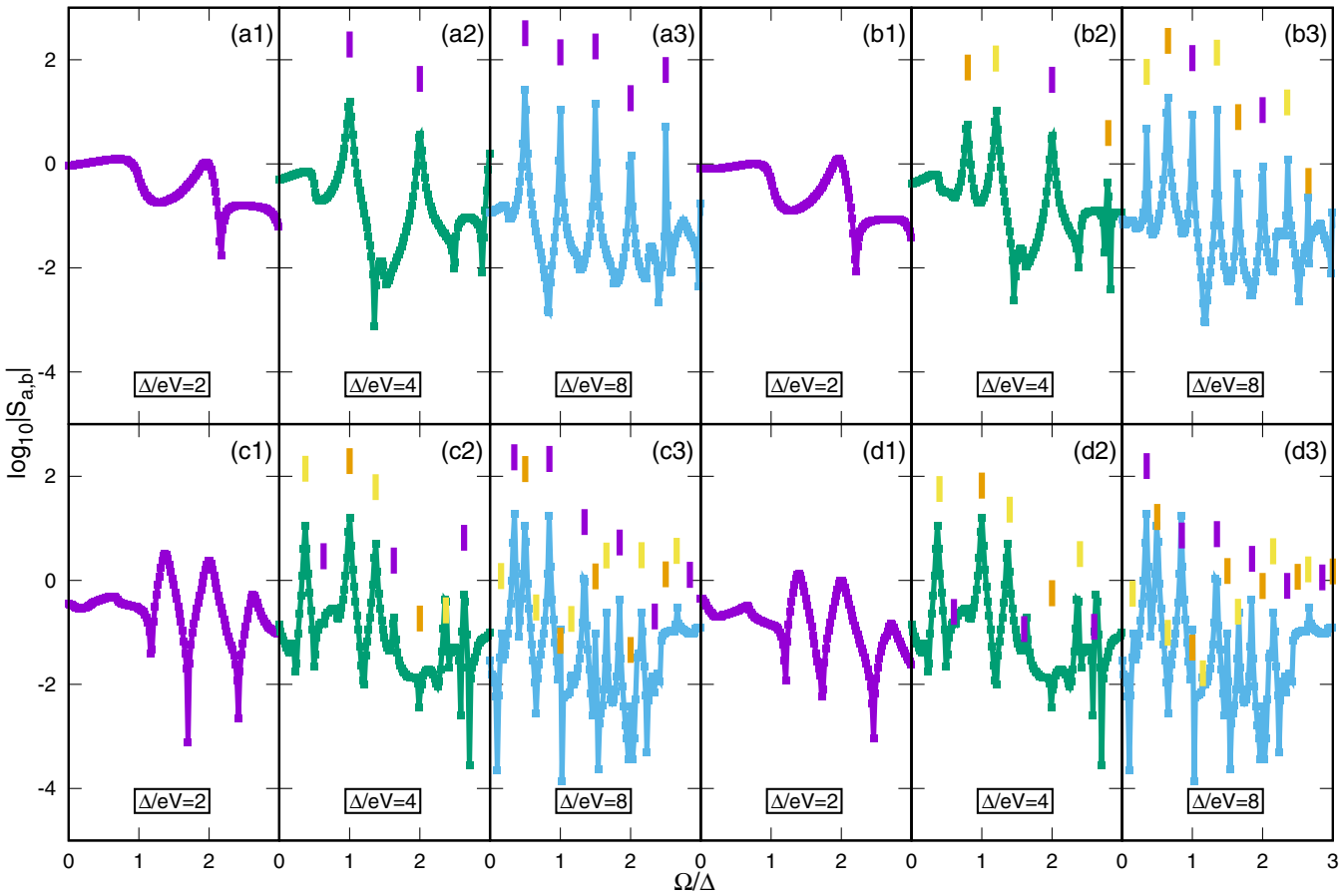

FIG. 6. Cross-correlation spectra $\log_{10}|S_{a,b}(\Omega)|$. The same as Fig. 5 but now y axis (i.e., the $S_{a,b}$ axis) is a logarithmic scale. Temperature is vanishingly small.

theoretically predicted peaks are barely visible in $S_{a,b}(\Omega)$ (see Fig. 5) or $\log_{10}|S_{a,b}(\Omega)|$ (see Fig. 6), because they are directly surrounded by sharp peaks with positive and negative signs, and thus, the value $|S_{a,b}|$ is weak for these resonances.

Panels (a1)–(d1) of Fig. 7 show the cross-correlations $S_{a,b}(\Delta/eV, \Omega/eV)$ in the plane of parameters Δ/eV (on x axis) and Ω/eV (on y axis). This is compared with panels (a2)–(d2) on the same figure, featuring $(E_n - E_m)/eV$ (on y axis) as a function of inverse voltage Δ/eV (on x axis). The data for the resolvent are similar to those in Fig. 4, but now in the experimentally relevant window $2 \lesssim \Delta/eV \lesssim 10$ of inverse voltage. The data on panels (a2)–(d2) were truncated to $\Delta/eV \geqslant 5$. The values of E_n and E_m calculated from $|\mathscr{R}(E)|$ are indeed within the gap region $-\Delta \lesssim E_n,\ E_m \lesssim \Delta$. This implies lower bound on Δ/eV if one wants to produce from $|\mathscr{R}(E)|$ the full spectrum of $(E_n - E_m)/eV$ within range $0 < (E_n - E_m)/eV < 16$ [see panels (a2)–(d2) of Fig. 7].

We note also the presence in Fig. 7(d1) of a resonance line at frequency $\Omega = 2\Delta$, in addition to the FWS resonance lines coinciding with Fig. 7(d2). This resonance corresponds to the expected transitions between both gap edge singularities at energies $\pm\Delta$. The resulting peak in $S_{a,b}$ cannot be distinguished from the series of transitions between FWS ladders in the preceding Figs. 5 and 6, because Δ/eV is an integer on these figures, implying that the quasiparticle resonance at energy 2Δ necessarily coincides with the transitions $\Delta E_{0,p}$ [see Eq. (4)].

It is concluded from Figs. 5–7 that the frequency Ω of the sharp peaks in the cross-correlation matches very well the energy difference $E_n - E_m$ between FWS resonances in the resolvent, in addition to a quasiparticle line at energy $\Omega = 2\Delta$. This confirms that finite frequency cross-correlations can be used to make spectroscopy of the Floquet spectrum (i.e., the spectrum of the FWS ladders) in a multiterminal superconducting-QD. Our predictions for the voltage dependence is of particular relevance to experiments, which is discussed now in the concluding section.

V. SUMMARY AND PERSPECTIVES

A. Summary

The equilibrium ABS are protected by a finite energy gap from the semi-infinite quasiparticle continua in multiterminal superconducting-QD. The nonequilibrium Floquet states can thus have very long lifetime. Still, the higher-order MAR provide a finite width γ to these FWS resonances, which is exponentially small in Δ/eV. Due to the drastic reduction of γ as eV/Δ decreases, sharp resonances emerge already in a relatively large range of $eV/\Delta \lesssim 1/3$ (see Figs. 5 and 6 for the evolution with voltage of the width of the resonances in the cross-correlations).

An analytical theory was presented, which takes advantage of the smallness of the width of the FWS resonances. A compact expression was obtained for the charge-charge

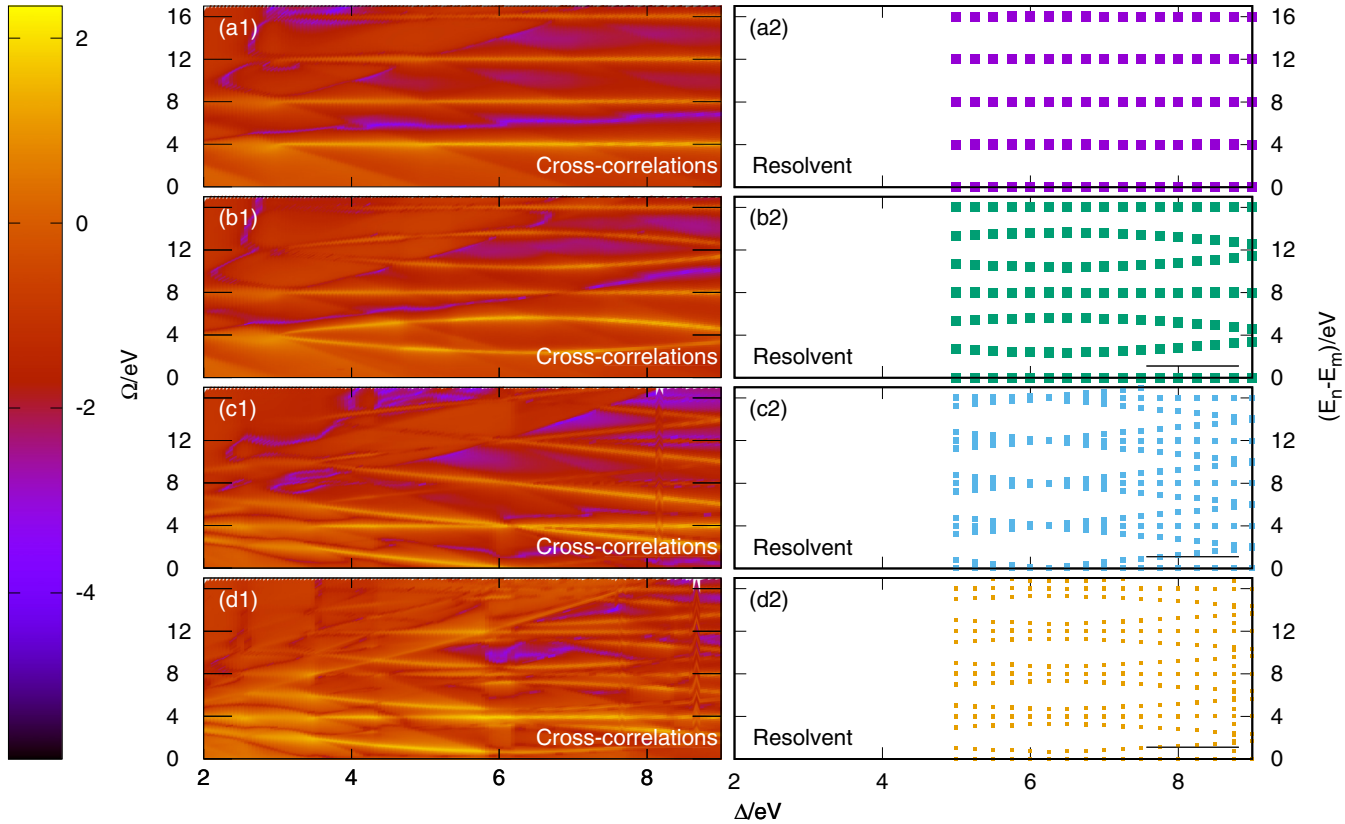

FIG. 7. Comparison between the cross-correlation and resolvent spectra. The contact transparencies are given in Table II: [(a1) and (a2)] two symmetrically coupled terminals, $\Gamma_a/\Delta = \Gamma_b/\Delta = 0.3$; [(b1) and (b2)] two terminals with generically different couplings to the leads, $\Gamma_a/\Delta = 0.4$, $\Gamma_b/\Delta = 0.2$; [(c1) and (c2)] three symmetrically coupled terminals with vanishingly small quartet phase $\varphi_q/2\pi = 0$, $\Gamma_a/\Delta = \Gamma_b/\Delta = \Gamma_c/\Delta = 0.3$; and [(d1) and (d2)] three symmetrically coupled terminals with finite value for the quartet phase $\varphi_q/2\pi = 0.1$, $\Gamma_a/\Delta = \Gamma_b/\Delta = \Gamma_c/\Delta = 0.3$. (a1), (b1), (c1), and (d1) show $\log_{10}|S_{a,b}(eV/\Delta, \Omega/\Delta)|$ (the logarithm of the cross-correlations) in color scale, as a function of normalized inverse voltage Δ/eV (x axis) and normalized frequency Ω/eV (y axis). (a2), (b2), (c2), and (d2) show the theoretical prediction [see Eqs. (3)–(5)], i.e., the collection of $(E_n - E_m)/eV$ vs Δ/eV, where E_n and E_m are two arbitrary Floquet energies. The bright peaks in the color-plot in (a1)–(d1) correspond to the peaks in the cross-correlations, also visible in Figs. 5 and 6. Similar inverse-voltage dependence is obtained for the calculated cross-correlations [see (a1)–(d1)] and the Floquet spectrum (i.e., the collection of $(E_n - E_m)/eV$) [see (a2)–(d2)]. The dark blue areas in (a1)–(d1) correspond to the regions in which the cross-correlations $S_{a,b}$ is small in absolute value (thus with negative $\log_{10}|S_{a,b}|$), due to change of sign of $S_{a,b}$ as a function of Ω between some of the resonance peaks (see Fig. 5). Temperature is vanishingly small.

correlation function. Remarkably, due to the presence of sharp FWS resonances, the charge correlation function factorizes into a product of two quantities: (i) a first term containing information about the populations in the lead and (ii) a second one involving products of four Floquet wave functions on the QD. This analytical theory reveals three series of peaks in the frequency dependence of the cross-correlations, which receive interpretation of transitions between Floquet states belonging to the same or different ladder. Numerical calculations for the cross-correlations $S_{a,b}$ (between currents entering the superconducting leads S_a and S_b) were presented in the case of two- and three-terminal configurations with various symmetries of the couplings. The numerical results for the location in energy of the resonances are in a quantitative agreement with the analytical theory. It is concluded that the nontrivial voltage dependence of the Floquet spectrum can be accessed experimentally *via* finite frequency noise spectroscopy in a superconducting-QD.

B. Perspectives

Calculating the nonsymmetrized correlators instead of the symmetrized ones would not change the energy values of the peaks in the noise, but may possibly modify their sign. This question will be addressed in the future in connection with experiments.

Expanding the modulus square in Eq. (13) produces several terms in which different physical processes can be recognized. It would be interesting to investigate a similar expansion for the current cross-correlations. Classifying the different processes beyond perturbation theory was already done for the dc-current [70] and for the current cross-correlations [71–75] of a metallic normal metal-superconducting-normal metal double junction. For a multiterminal all-superconducting-QD (see Fig. 1), this can lead to nonperturbative characterization of the quartet [18,19,25], multipair or phase-MAR [19,20,26] channels. At present time, separation of the dc-current [26] and the current-current cross-correlations [28] into the

different physical channels relies solely on the symmetries with respect to phase or voltage inversion [22].

Another interesting perspective is to develop nonstandard algorithms to calculate the current and the current-current correlation function in the sharp resonance approximation. Namely, this approximation is based on a limited number of parameters for the spectrum of FWS resonances (i.e., the position of the Floquet resonance energies and their width), and on the Floquet wave functions at resonance. The factorized form of the charge-charge correlation function [see Eq. (12)] suggests the possibility of spectacular enhancement of the performances of the codes with respect to those used in Sec. IV C to evaluate the current correlation functions.

It is also an open question to show that FWS ladders are robust against Coulomb interaction. We note that finite frequency noise has been calculated recently for an interacting quantum dot [76].

Figures 7(b1) and 7(b2) reveal nontrivial features already for a two-terminal device with generically different couplings to the leads in the experimentally accessible voltage range $0.1 \lesssim eV/\Delta \lesssim 1$. Two-terminal devices are much easier to control experimentally than their three-terminal counterparts. Figures 7(b1) and 7(b2) feature repulsion among FWS resonances in this case, which is a signature of quantum coherent coupling between the time-periodic states originating from different ladders. The Floquet wave functions are then delocalized on both "FWS ladder rungs" in quasicoincidence (as a function of the coordinate N in Fig. 3). Future perspectives on a "Floquet qu-bit" based on the time-periodic dynamics of the superconducting-QD can be envisioned, including opening on the physics of driven qu-bits [77,78]. Finally, the possibility to perform tunnel spectroscopy of the FWS ladders is currently under investigation.

ACKNOWLEDGMENTS

The authors thank the Centre Régional Informatique et d'Applications Numériques de Normandie (CRIANN) for the use of its facilities. The authors thank the Infrastructure de Calcul Intensif et de Données (GRICAD) for use of the resources of the Mésocentre de Calcul Intensif de l'Université Grenoble-Alpes (CIMENT). R.M. and R.D. acknowledge financial support from the Centre National de la Recherche Scientifique (CNRS) and Karlsruhe Institute of Technology (KIT), through the International Laboratory "LIA SUPRADEVMAT" between the Grenoble and Karlsruhe campuses. This work was partly supported by Helmholtz society through program STN and the DFG via the Projects DA 1280/3-1.

[1] A. Zazunov, V. S. Shumeiko, E. N. Bratus', J. Lantz, and G. Wendin, Andreev Level Qubit, Phys. Rev. Lett. **90**, 087003 (2003).

[2] A. F. Andreev, The thermal conductivity of the intermediate state in superconductors, Zh. Eksp. Teor. Fiz. **46**, 1823 (1964) [Sov. Phys. JETP **19**, 1228 (1964)].

[3] P. G. de Gennes and D. Saint-James, Elementary excitations in the vicinity of a normal metal-superconducting metal contact, Phys. Lett. **4**, 151 (1963).

[4] D. Saint-James, Excitations élémentaires au voisinage de la surface de séparation d'un métal normal et d'un métal supraconducteur, J. Phys. (Paris) **25**, 899 (1964).

[5] I. O. Kulik, Macroscopic quantization and the proximity effect in SNS junctions, Zh. Eksp. Teor. Fiz. **57**, 1745 (1970) [Sov. Phys. JETP **30**, 944 (1970)].

[6] A. Yu. Kitaev, Unpaired majorana fermions in quantum wires, Phys. Usp. **44**, 131 (2001).

[7] V. Mourik, K. Zuo, S. M. Frolov, S. R. Plissard, E. P. A. M. Bakkers, and L. P. Kouwenhoven, Signatures of Majorana fermions in hybrid superconductor-semiconductor nanowire devices, Science **336**, 1003 (2012).

[8] Y. Huang, H. Pan, C.-X. Liu, J. D. Sau, T. D. Stanescu, and S. Das Sarma, Metamorphosis of Andreev bound states into Majorana bound states in pristine nanowires, Phys. Rev. B **98**, 144511 (2018).

[9] D. M. Badiane, M. Houzet, and J. S. Meyer, Nonequilibrium Josephson Effect Through Helical Edge States, Phys. Rev. Lett. **107**, 177002 (2011).

[10] M. Houzet, J. S. Meyer, D. M. Badiane, and L. I. Glazman, Dynamics of Majorana States in a Topological Josephson Junction, Phys. Rev. Lett. **111**, 046401 (2013).

[11] D. M. Badiane, L. I. Glazman, M. Houzet, and J. S. Meyer, Ac Josephson effect in topological Josephson junctions, C. R. Phys. **14**, 840 (2013).

[12] B. van Heck, S. Mi, and A. R. Akhmerov, Single fermion manipulation via superconducting phase differences in multiterminal Josephson junctions, Phys. Rev. B **90**, 155450 (2014).

[13] C. Padurariu, T. Jonckheere, J. Rech, R. Mélin, D. Feinberg, T. Martin, and Y. V. Nazarov, Closing the proximity gap in a metallic Josephson junction between three superconductors, Phys. Rev. B **92**, 205409 (2015).

[14] R.-P. Riwar, M. Houzet, J. S. Meyer, and Y. V. Nazarov, Multi-terminal Josephson junctions as topological materials, Nat. Commun. **7**, 11167 (2016).

[15] E. Strambini, S. D'Ambrosio, F. Vischi, F. S. Bergeret, Y. V. Nazarov, and F. Giazotto, The ω-SQUIPT as a tool to phase-engineer Josephson topological materials, Nat. Nanotechnol. **11**, 1055 (2016).

[16] A. W. Draelos, M.-T. Wei, A. Seredinski, H. Li, Y. Mehta, K. Watanabe, T. Taniguchi, I. V. Borzenets, F. Amet, and G. Finkelstein, Supercurrent flow in multiterminal graphene Josephson junctions, Nano Lett. **19**, 1039 (2019).

[17] N. Pankratova, H. Lee, R. Kuzmin, M. Vavilov, K. Wickramasinghe, W. Mayer, J. Yuan, J. Shabani, and V. E. Manucharyan, The multi-terminal Josephson effect, arXiv:1812.06017.

[18] A. H. Pfeffer, J. E. Duvauchelle, H. Courtois, R. Mélin, D. Feinberg, and F. Lefloch, Subgap structure in the conductance of a three-terminal Josephson junction, Phys. Rev. B **90**, 075401 (2014).

[19] Y. Cohen, Y. Ronen, J. H. Kang, M. Heiblum, D. Feinberg, R. Mélin, and H. Strikman, Non-local supercurrent of quartets in a

three-terminal Josephson junction, Proc. Natl. Acad. Sci. USA **115**, 6991 (2018).
[20] Evidence for the thresholds of multiterminal Andreev reflection can be found in arXiv:1606.08436v2, the arXiv version of Ref. [19].
[21] M. Houzet and P. Samuelsson, Multiple Andreev reflections in hybrid multiterminal junctions, Phys. Rev. B **82**, 060517(R) (2010).
[22] R. Mélin, D. Feinberg, and B. Douçot, Partially resummed perturbation theory for multiple Andreev reflections in a short three-terminal Josephson junction, Eur. Phys. J. B **89**, 67 (2016).
[23] M. P. Nowak, M. Wimmer, and A. R. Akhmerov, Supercurrent carried by non-equlibrium quasiparticles in a multiterminal Josephson junction, Phys. Rev. B **99**, 075416 (2019).
[24] J. C. Cuevas and H. Pothier, Voltage-induced Shapiro steps in a superconducting multiterminal structure, Phys. Rev. B **75**, 174513 (2007).
[25] A. Freyn, B. Douçot, D. Feinberg, and R. Mélin, Production of Non-Local Quartets and Phase-Sensitive Entanglement in a Superconducting Beam Splitter, Phys. Rev. Lett. **106**, 257005 (2011).
[26] T. Jonckheere, J. Rech, T. Martin, B. Douçot, D. Feinberg, and R. Mélin, Multipair dc Josephson resonances in a biased all-superconducting bijunction, Phys. Rev. B **87**, 214501 (2013).
[27] J. Rech, T. Jonckheere, T. Martin, B. Douçot, D. Feinberg, and R. Mélin, Proposal for the observation of nonlocal multipair production, Phys. Rev. B **90**, 075419 (2014).
[28] R. Mélin, M. Sotto, D. Feinberg, J.-G. Caputo, and B. Douçot, Gate-tunable zero-frequency current cross-correlations of the quartet mode in a voltage-biased three-terminal Josephson junction, Phys. Rev. B **93**, 115436 (2016).
[29] S. Mai, E. Kandelaki, A. Volkov, and K. Efetov, Stationary Josephson effect in a short multiterminal junction, Phys. Rev. B **87**, 024507 (2013).
[30] A. Murani, A. Chepelianskii, S. Guéron, and H. Bouchiat, Andreev spectrum with high spin-orbit interactions: Revealing spin splitting and topologically protected crossings, Phys. Rev. B **96**, 165415 (2017).
[31] J.-D. Pillet, V. Benzoni, J. Griesmar, J.-L. Smirr, and Ç. Ö. Girit, Non-local Josephson effect in Andreev molecules, arXiv:1809.11011.
[32] J.-D. Pillet, C. H. L. Quay, P. Morfin, C. Bena, A. Levy Yeyati, and P. Joyez, Revealing the electronic structure of a carbon nanotube carrying a supercurrent, Nat. Phys. **6**, 965 (2010).
[33] T. Dirks, T. L. Hughes, S. Lal, B. Uchoa, Y.-F. Chen, C. Chialvo, P. M. Goldbart, and N. Mason, Transport through Andreev bound states in a graphene quantum dot, Nat. Phys. **7**, 387 (2011).
[34] L. Bretheau, Ç. Ö. Girit, D. Esteve, H. Pothier, and C. Urbina, Tunnelling spectroscopy of Andreev states in graphene, Nature (London) **499**, 312 (2013).
[35] L. Bretheau, Ç. Ö. Girit, C. Urbina, D. Esteve, and H. Pothier, Supercurrent Spectroscopy of Andreev States, Phys. Rev. X **3**, 041034 (2013).
[36] J. Schindele, A. Baumgartner, R. Maurand, M. Weiss, and C. Schönenberger, Nonlocal spectroscopy of Andreev bound states, Phys. Rev. B **89**, 045422 (2014).
[37] D. G. Olivares, A. Levy Yeyati, L. Bretheau, Ç. Ö. Girit, H. Pothier, D. Esteve, and C. Urbina, Dynamics of quasiparticle trapping in Andreev levels, Phys. Rev. B **89**, 104504 (2014).
[38] C. Janvier, L. Tosi, L. Bretheau, Ç. Ö. Girit, M. Stern, P. Bertet, P. Joyez, D. Vion, D. Esteve, M. F. Goffman, H. Pothier, and C. Urbina, Coherent manipulation of Andreev states in superconducting atomic contacts, Science **349**, 1199 (2015).
[39] J. Gramich, A. Baumgartner, and C. Schönenberger, Resonant and Inelastic Andreev Tunneling Observed on a Carbon Nanotube Quantum Dot, Phys. Rev. Lett. **115**, 216801 (2015).
[40] L. Bretheau, J. I.-J. Wang, R. Pisoni, K. Watanabe, T. Taniguchi, and P. Jarillo-Herrero, Tunnelling spectroscopy of Andreev states in graphene, Nat. Phys. **13**, 756 (2017).
[41] J. Gramich, A. Baumgartner, and C. Schönenberger, Andreev bound states probed in three-terminal quantum dots, Phys. Rev. B **96**, 195418 (2017).
[42] B. Dassonneville, A. Murani, M. Ferrier, S. Guéron, and H. Bouchiat, Coherence-enhanced phase-dependent dissipation in long SNS Josephson junctions: Revealing Andreev bound state dynamics, Phys. Rev. B **97**, 184505 (2018).
[43] L. Tosi, C. Metzger, M. F. Goffman, C. Urbina, H. Pothier, S. Park, A. Levy Yeyati, J. Nygård, and P. Krogstrup, Spin-Orbit Splitting of Andreev States Revealed by Microwave Spectroscopy, Phys. Rev. X **9**, 011010 (2019).
[44] R. Mélin, J.-G. Caputo, K. Yang, and B. Douçot, Simple Floquet-Wannier-Stark-Andreev viewpoint and emergence of low-energy scales in a voltage-biased three-terminal Josephson junction, Phys. Rev. B **95**, 085415 (2017)
[45] G. H. Wannier, Wave-functions and effective Hamiltonian for Bloch electrons in an electric field, Phys. Rev. **117**, 432 (1960).
[46] E. E. Mendez, F. Agullo-Rueda, and J. M. Hong, Stark Localization in GaAs-GaAlAs Superlattices under an Electric Field, Phys. Rev. Lett. **60**, 2426 (1988).
[47] E. E. Mendez and G. Bastard, Wannier-Stark ladders and Bloch oscillations in superlattices, Phys. Today **46**(6), 34 (1993).
[48] P. W. Anderson, Consideration on the flow of superfluid helium, Rev. Mod. Phys. **38**, 298 (1966).
[49] P. W. Anderson, The Josephson effect and quantum coherence measurements in superconductors and superfluids, Prog. Low Temp. Phys. **5**, 1 (1967).
[50] F. Bloch, Über die Quantenmechanik der Elektronen in Kristallgittern, Z. Phys. **52**, 555 (1928).
[51] C. Zener, A theory of the electrical breakdown of solid dielectrics, Proc. R. Soc. London A **145**, 523 (1934).
[52] L. Esaki and R. Tsu, Superlattice and negative differential conductivity in semiconductors, IBM J. Res. Develop. **14**, 61 (1970).
[53] S. R. Wilkinson, C. F. Bharucha, K. W. Madison, Q. Niu, and M. G. Raizen, Observation of Atomic Wannier-Stark Ladders in an Accelerating Optical Potential, Phys. Rev. Lett. **76**, 4512 (1996).
[54] M. Ben Dahan, P. Ekkehard, J. Reichel, Y. Castin, and C. Salomon, Bloch Oscillations of Atoms in an Optical Potential, Phys. Rev. Lett. **76**, 4508 (1996).
[55] Z. A. Geiger, K. M. Fujiwara, K. Singh, R. Senaratne, S. V. Rajagopal, M. Lipatov, T. Shimasaki, R. Driben, V. V. Konotop, T. Meier, and D. M. Weld, Observation and Uses of Position-Space Bloch Oscillations in an Ultracold Gas, Phys. Rev. Lett. **120**, 213201 (2018).

[56] J. Delahaye, J. Hassel, R. Lindell, M. Silanpää, M. Paalanen, H. Seppä, and P. J. Hakonen, Low noise current amplifier based on mesoscopic Josephson junction, Science **299**, 1045 (2003).

[57] J. Sarkar, A. Puska, J. Hassel, and P. J. Hakonen, Differential Bloch oscillating transistor pair, Supercond. Sci. Technol. **26**, 065009 (2013).

[58] K. K. Likharev, Superconducting weak links, Rev. Mod. Phys. **51**, 101 (1979).

[59] K. Hino, X. M. Tong, and N. Toshima, Interacting dynamic Wannier-Stark ladder driven by a periodic pulse train, Phys. Rev. B **77**, 045322 (2008).

[60] D. Averin and A. Bardas, AC Josephson Effect in a Single Quantum Channel, Phys. Rev. Lett. **75**, 1831 (1995).

[61] J. C. Cuevas, A. Martín-Rodero, and A. Levy Yeyati, Hamiltonian approach to the transport properties of superconducting quantum point contacts, Phys. Rev. B **54**, 7366 (1996).

[62] E. Scheer, N. Agraït, J. C. Cuevas, A. Levy Yeyati, B. Ludophk, A. Martín-Rodero, G. Rubio Bollinger, J. M. van Ruitenbeekk, and C. Urbina, The signature of chemical valence in the electrical conduction through a single-atom contact, Nature (London) **394**, 154 (1998).

[63] C. W. Beenakker, in *Proceedings of the 14th Taniguchi International Symposium on Transport Phenomena in Mesoscopic Systems*, edited by H. Fukuyama and T. Ando (Springer, Berlin, 1992).

[64] See Supplemental Material at http://link.aps.org/supplemental/10.1103/PhysRevB.100.035450 for technical details of the analytical calculations.

[65] F. Bentosela, V. Grecchi, and F. Zironi, Oscillations of Wannier Resonances, Phys. Rev. Lett. **50**, 84 (1983).

[66] L. D. Landau and E. M. Lifshitz, *Quantum Mechanics*, 3rd ed. (Elsevier, Amsterdam, 1981).

[67] S. N. Shevchenko, S. Ashhab, and F. Nori, Landau-Zener-Stückelberg interferometry, Phys. Rep. **492**, 1 (2010).

[68] J. C. Cuevas, A. Martín-Rodero, and A. Levy Yeyati, Shot Noise and Coherent Multiple Charge Transfer in Superconducting Quantum Point Contacts, Phys. Rev. Lett. **82**, 4086 (1999).

[69] R. Cron, M. F. Goffman, D. Esteve, and C. Urbina, Multiple-Charge-Quanta Shot Noise in Superconducting Atomic Contacts, Phys. Rev. Lett. **86**, 4104 (2001).

[70] R. Mélin and D. Feinberg, Sign of the crossed conductance at a ferromagnet/superconductor/ferromagnet double interface, Phys. Rev. B **70**, 174509 (2004).

[71] R. Mélin, C. Benjamin, and T. Martin, Positive cross correlations of noise in superconducting hybrid structures: Roles of interfaces and interactions, Phys. Rev. B **77**, 094512 (2008).

[72] D. S. Golubev and A. D. Zaikin, Shot noise and Coulomb effects on nonlocal electron transport in normal-metal/superconductor/normal-metal heterostructures, Phys. Rev. B **82**, 134508 (2010).

[73] A. Freyn, M. Flöser, and R. Mélin, Positive current cross-correlations in a highly transparent normal-superconducting beam splitter due to synchronized Andreev and inverse Andreev reflections, Phys. Rev. B **82**, 014510 (2010).

[74] M. Flöser, D. Feinberg, and R. Mélin, Absence of split pairs in cross correlations of a highly transparent normal metal-superconductor-normal metal electron-beam splitter, Phys. Rev. B **88**, 094517 (2013).

[75] D. S. Golubev and A. Zaikin, Cross-correlated shot noise in three-terminal superconducting hybrid nanostructures, Phys. Rev. B **99**, 144504 (2019).

[76] A. Crépieux, S. Sahoo, T. Q. Duong, R. Zamoum, and M. Lavagna, Emission Noise in an Interacting Quantum Dot: Role of Inelastic Scattering and Asymmetric Coupling to the Reservoirs, Phys. Rev. Lett. **120**, 107702 (2018).

[77] P. J. Leek, J. M. Fink, A. Blais, R. Bianchetti, M. Göppl, J. M. Gambetta, D. I. Schuster, L. Frunzio, R. J. Schoelkopf, and A. Wallraff, Observation of Berry's phase in a solid state qubit, Science **318**, 1889 (2007).

[78] K. W. Murch, U. Vool, D. Zhou, S. J. Weber, S. M. Girvin, and I. Siddiqi, Cavity-Assisted Quantum Bath Engineering, Phys. Rev. Lett. **109**, 183602 (2012).